Source Mechanism Study of Quetta Earthquake of May 30, 1935

HARSH K. GUPTA and D. D. SINGH

Abstract: The source mechanism of the major destructive earthquake which occurred in the Quetta region on May 30, 1935 is determined using the P-wave first motions, S-wave polarization angles and surface waves spectral data. A thrust faulting is obtained along a plane with strike N 33°E, dip 68°NW, slip angle 124° and a focal depth of 20 km. A unilateral fault of about 106 km, rupturing with a velocity of 3.1 km/sec is obtained from the differential phase and the directivity function of G2 — G3 and R2 — R3 waves. The source parameters obtained from the surface waves spectra are: seismic moment = 1.75×10^{28} dyne-cm; dislocation = 32.81 meters; fault area = 1778 sq. km; apparent stress = 283 bars; stress drop = 567 bars; strain energy = 1.65×10^{25} ergs and strain drop = 18.9×10^{-4}. The high stress drop and apparent stress associated with this event suggest that high tectonic stresses are prevailing in this region. A major part of the stresses accumulated before the occurrence of this earthquake had been released through the main shock.

INTRODUCTION

Himalayan frontal arc, flanked by the Chaman fault in the west and Arakanyoma in the east, is seismically one of the most active region in the entire Alpine belt. Fig. 1 shows the epicenters of major earthquakes since 1897 of magnitude ⩾ 7.5, that have occurred in the region. Some of these earthquakes were very

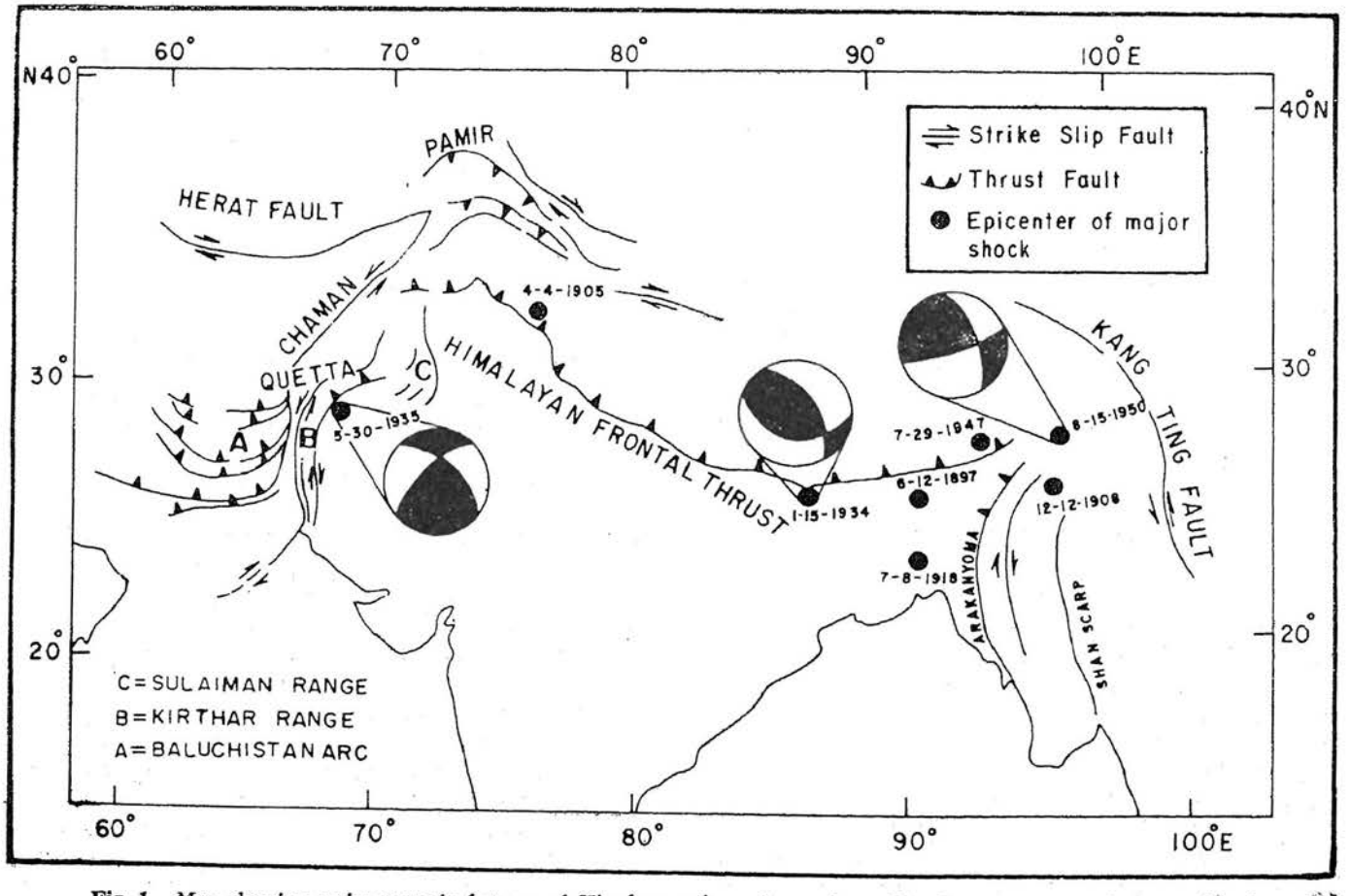

Fig. 1. Map showing major tectonic features of Himalaya and nearby regions. The dots represent epicenters of major earthquakes since 1897. The mechanism solution for the 1950 earthquake has been taken from Ben-Menahem *et al.* (1974). Solutions for the 1934 and 1935 earthquakes are also shown (Singh and Gupta, 1980).

Proc. Intern. Commit. Geodynamics, Grp. 6, Mtg. Peshawar, Nov. 23-29, 1979: Spec. Issue, Geol. Bull. Univ. Peshawar, Vol. 13, 1980.

damaging and claimed thousands of human lives. The focal mechanism solutions provide better means for determining the orientation of regional stress, nature of faulting and sense of motion on the faults. The focal mechanism solutions for a very few large magnitude earthquakes are available in the Himalayan and nearby regions. For understanding the regional tectonics of the region, it is necessary to know the source parameters of these earthquakes. Ben-Menahem *et al.* (1974) investigated in detail the Assam earthquake of August 15, 1950. The source parameters of the Bihar-Nepal earthquake of January 15, 1934 have been investigated in detail by Singh and Gupta (1980). Among the remaining earthquakes, the Quetta earthquake of May 30, 1935 is of special interest, as sufficient instrumental data are available to carry out the detailed source parameter studies.

The area surrounding the Quetta syntaxis forms one of the seismically most active region in the Alpine belt. Several earthquakes have occurred in the pre-historical times causing severe damage to both property and life. The focal mechanism solution for earthquakes occuring in this region has been determined by various investigators like Quittmeyer *et al.* (1979) and Chandra (1978 and 1980). A major destructive earthquake of magnitude M = 7.6 occurred close to (Fig. 1) Quetta (epicenter 29.5°N, 66.7°E) on May 30, 1935 (origin time 21 h 33 m 0.0. s). It caused a considerable amount of destruction, claimed an estimated 30,000 human lives and created numerous fractures and landslides. Here we present the detailed source parameter investigations for this earthquake using the available records of different seismological stations throughout the world. The focal mechanism and different seismic source parameters like fault length, rupture velocity, source time function, seismic moment, dislocation, apparent stress, stress and strain drop are estimated using the body and surface waves data of this earthquake.

FOCAL MECHANISM

P and S waves data: Seismograms were obtained for the Quetta earthquake from different seismological stations throughout the world. The P-wave first motion directions are read from the long period vertical component records. These first motions are plotted on the lower hemisphere of the equal area projection (Fig. 2). S-wave polarization angles are determined using the records of a few seismic stations. These are plotted in Fig. 2. The standard deviation and average error are calculated by varying the dip and strike of the nodal planes within the range, which were permitted from the P-wave data. For the best fit model, the standard deviation and average error are estimated to be 10.6° and 8.8°. Here the P and S waves data are not sufficient for defining the nodal planes accurately

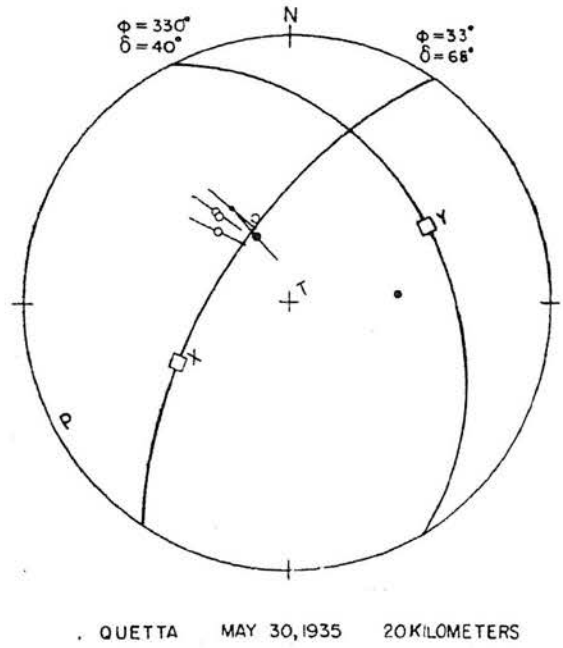

Fig. 2. Fault plane solution determined using first motions read from long-period records. Filled and open circles represent first motions compressions and dilatations, respectively. P is the pressure axis or axis of maximum compression, T is the tension axis or axis of minimum compression. X and Y are the poles of the two nodal planes. S-wave polarization directions are shown by short lines. Small dots indicate stations for which only S-wave data are used.

and, therefore, surface waves spectral data have also been used.

Rayleigh/Love wave spectral ratio: Surface wave spectral ratio has advantages over the use of absolute surface waves spectra, as we do not have to apply the corrections for the effect of instrument, path, source finiteness and source time function (Canitez and Toksoz, 1971). For the determination of observed spectral ratio, the fundamental mode Rayleigh and Love waves of several minutes duration (Fig. 3 and Table 1) are digitized at the varying time intervals, depending upon the wave forms. These data are then interpolated at a fixed time interval of 0.3 sec using the Lagerangian interpolation method. The digitized data are detrended and the arithmetic mean is removed. Afterwards, the data are Fourier analysed using the Simpson's method to get the spectral amplitude and phase. The theoretical spectral ratios are calculated using the method of Harkrider (1970) for different fault orientations consistent with the P- and S-waves data. The best fit is obtained by the trial and error comparison of the observed Rayleigh/Love wave spectral ratio with the theoretical ones, calculated for focal depths of 10, 20 and 35 km at five seismic stations. A few such plots are shown in Fig. 4 for the selected best fit model. The fault

TABLE I. The Digitized Signals Recorded at Different Seismic Stations for the Quetta earthquake of May 30, 1935.

Station	Seismograph Name	Component	Wave	Distance (km)	Beginning of the time window GMT			End of the time window GMT		
					hr	min	sec	hr	min	sec
Uppsala	Wiechert	EW	LQ	4933	21	51	24	22	00	28
Copenhagen	Wiechert	Z	LR	5099	21	55	06	22	12	30
		EW	LQ	5099	21	52	30	22	04	56
		NS	LQ	5099	21	52	08	22	00	00
	Galitzin Wilip	Z	LR	5099	21	54	30	22	02	42
		EW	G2	34897	23	40	54	23	50	36
		EW	G3	45095	01	17	18	01	24	00
Stuttgart	Galitzin Willip	Z	R2	34763	23	35	04	23	42	06
		Z	R3	45229	00	23	12	00	29	44
		EW	G2	34763	23	35	00	23	43	16
		EW	G3	45229	00	20	30	00	28	52
		NS	G2	34763	23	38	00	23	45	50
		NS	G3	45229	00	20	46	00	27	24
Scoresbysund	Galitzin Wilip	NS	LQ	6855	21	59	28	22	09	18
		Z	LR	6855	22	02	18	22	20	46
		NS	G2	33141	23	34	44	23	45	12
		NS	G3	46851	00	26	04	00	36	40
		Z	R2	33141	23	46	48	23	58	34
		Z	R3	46851	00	37	16	00	44	00
Ivigtut	Wiechert	NS	LQ	8344	22	05	24	22	21	08
		EW	LQ	8344	22	05	28	22	20	04
		Z	LR	8344	22	08	40	22	30	40
Melbourne	Milne Shaw	NS	LQ	11054	22	14	32	22	30	34
Wellington	Milne Shaw	NS	LQ	13565	22	27	04	22	45	00
		Z	LR	13565	22	35	00	22	50	00

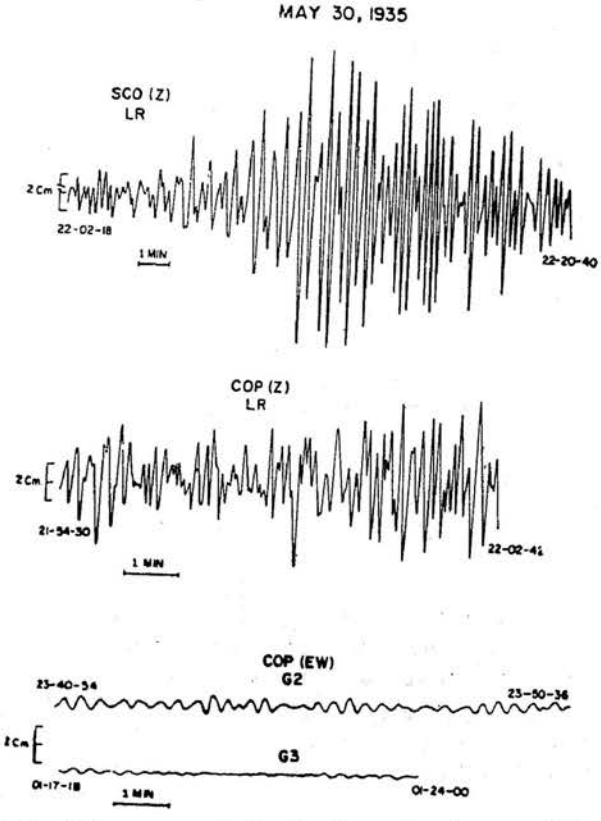

Fig. 3. Seismograms of the Quetta earthquake recorded at few seismic stations.

plane orientation for the best fit model are as follows:

Strike, Φ = N33°E

Dip, δ = 68°NW

Slip angle, λ = 124°

Focal depth, H = 20 km

Fault length, rupture velocity and source time function: Directivity function was defined by Ben-Menahem (1961) as the ratio of the spectral amplitude of waves leaving the source in opposite directions:

$$D = \frac{\left| \left(\frac{c}{v} + \mathrm{Cos}\Theta\right) \left[\mathrm{Sin}\frac{\pi bf}{c}\left(\frac{c}{v} - \mathrm{Cos}\Theta\right)\right] \right|}{\left| \left(\frac{c}{v} - \mathrm{Cos}\Theta\right) \left[\mathrm{Sin}\frac{\pi bf}{c}\left(\frac{c}{v} + \mathrm{Cos}\Theta\right)\right] \right|}$$

where

c = phase velocity

b = fault length

v = rupture velocity

Θ = angle between the fault plane and the great circle from the fault to the recording station.

TABLE 2. Estimates of the Fault Length for Quetta earthquake of May 30, 1935 from the Differential Phases of Love and Rayleigh waves

Frequency (Hz)	Period (Sec.)	STU (G2/G3)	SCO (R2/R3)
0.00569	175.5	33	76
0.00732	136.5	38	97
0.00895	111.7	29	72
0.01058	94.5	11	61
0.01221	81.9	13	64
0.01383	72.3	21	52
0.01546	64.7	11	43
0.01709	58.5	29	47
0.01872	53.4	15	51
0.02035	49.2	22	59
0.02197	45.5	14	47

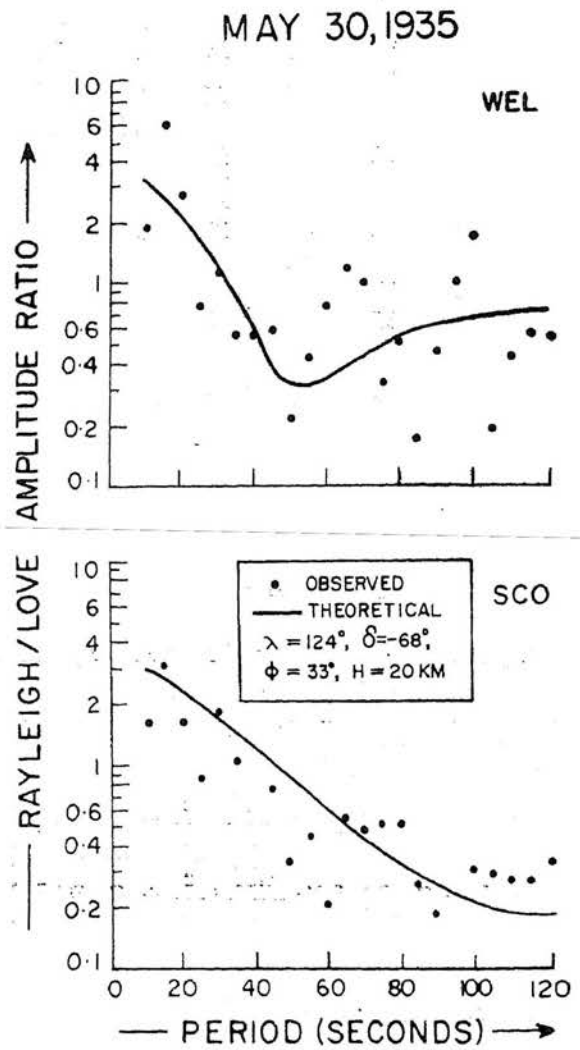

Fig. 4. Comparison of observed Rayleigh/Love wave spectral ratio (dots) with the theoretical ones (continuous line) at a few stations for the best fit model.

We have estimated the fault length and rupture velocity from the differential phases and the directivity function method (Ben-Menahem and Toksöz, 1962 and 1963). For the determination of differential phases of G2–G3 and R2–R3, the Love and Rayleigh waves for Quetta earthquake are digitized (Fig. 3 and Table 1) as described earlier. The digitized data are detrended, corrected for amplitude and instrumental phase shift (Hagiwara, 1958). The amplitude and phase spectrum are obtained using the fast Fourier transform algorithem. The initial phase is obtained using the relation of Ben-Menahem and Toksöz (1962):

$$\Phi_o = f t_n + \Phi' + \Phi_{inst} - f\frac{\Delta}{c} - (M + \tfrac{1}{2})$$

where

f = frequency

t_n = the time lag of the beginning of the spectral window with respect to the origin time.

Φ' = Fourier phase

Δ = epicentral distance of the recording station

M = an integer

Φ_{inst} = instrumental phase shift

The initial phase, Φ_o, is corrected for the source finiteness effect. Then the differential phase, $\delta\Phi_o$, is calculated for the pairs of R2–R3 and G2–G3 waves and is listed in Table 2. The average value of $\lambda'\delta\Phi_o$ (λ' = wave length) is estimated, which yields the fault length of 106 km.

The rupture velocity is calculated using the directivity functions of G2–G3 and R2–R3 waves. The observed directivity function is obtained from the spectral amplitude ratios of R2–R3 or G2–G3 waves, corrected for the absorption effect. The values of phase velocity and attenuation coefficients are taken from Mills and Hales (1978). The theoretical directivity is calculated from the above relation for different combinations of fault length and rupture velocity. The fault length is varied in the range of 106 ± 30 km and rupture velocity is varied from 2.5 to 3.5 km/sec. Fig. 5 shows the directivity functions for the selected best fit model. The rupture velocity is estimated to be 3.1 km/sec. We have also tried to match the observed directivity functions with the theoretical ones which were calculated for different seismic source models considered (Ben-Menahem and Toksöz, 1962). These are (i) the exponentially decaying source, and (ii) the bidirectional faulting. The theoretical directivity functions obtained for these two seismic source models do not match satisfactorily with the observed ones. The observed directivity function gives a better fit with the unilateral horizontal fault movement source model with

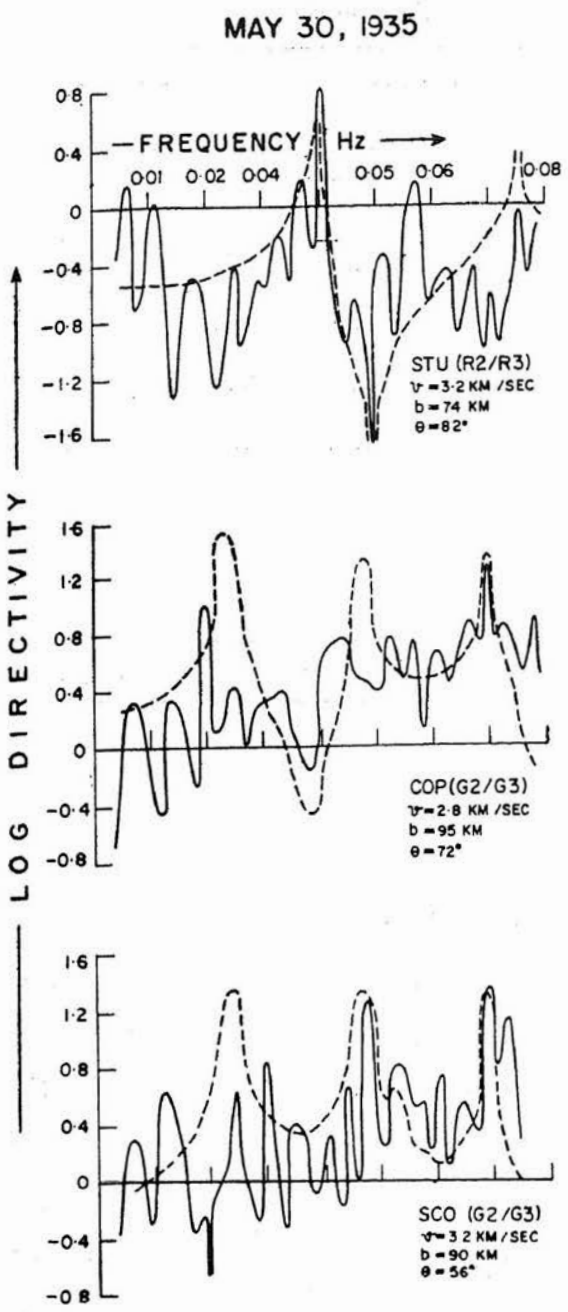

Fig. 5. Observed and theoretical values of directivity functions determined at different frequencies for the Quetta earthquake.

a constant rupture velocity. Therefore, unilateral fault propagation with a constant rupture propagation is inferred for Quetta earthquake.

Source time function is obtained using the initial phase of R2 waves. The initial phases of a seismic source are the phases of Fourier transform of its source time functions. For the synthesis of source time function, several trigonometrical and exponential functions, have been considered. The best fit is obtained by the trial and error methods of comparing the observed source time function with the synthesized ones. The source time function, which fits the observed data here satisfactorily, is written as:

$$G(t) = H(t)\{\log_{10}(1 + \frac{a^2}{t^2})\}$$

Here H (t) is the Heaviside unit step function and a is a constant. These results are shown in Fig. 6.

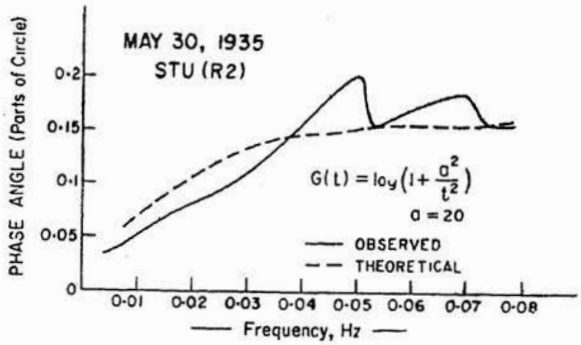

Fig. 6. The observed phase spectra of the source time function and the reconstructed source time of the Quetta earthquake.

Seismic moment and other source parameters: Seismic moment is a measure of the size of an earthquake source. We have determined it using the relation of Udias and Arroyo (1970). For the calculation of seismic moment, the spectral amplitudes which were determined earlier, have been used. We have corrected for the finiteness effect of the source by dividing by the factor Sin X/X,

where

$$X = b\,\omega\,(\frac{1}{v} - \text{Cos}\,\Theta/c)\,/2$$

The seismic moment values are listed in Table 3. Fault area, A, is determined from magnitude using the relation (Chinnery, 1969):

$$\log A\ (\text{Sq km}) = 0.60\ m - 1.31$$

After getting the fault length and fault area, we estimate the fault width, W, for a rectangular fault model. The average dislocation across the fault plane is estimated using the relation:

$$\bar{u} = \frac{M_o}{\mu A}$$

where

μ = shear modulus ($=3\times10^{11}$ dyne/cm^2)

TABLE 3. Seismic Moment Estimates for the Quetta earthquake of May 30, 1935.

Station	Distance (degree)	Rayleigh Wave M_o (10^{28} dyne-cm)		Love Wave M_o (10^{28} dyne-cm)			Average M_o (10^{28} dyne-cm)	
		110 sec	80 sec	65 sec	110 sec	80 sec	65 sec	
COP	45.9	4.87	3.08	1.32	2.76	2.15	2.76	2.82
SCO	61.7	3.53	1.67	1.32	4.71	1.20	4.72	2.86
IVI	75.1	1.57	0.38	0.22	0.59	0.35	0.51	0.60
WEL	122.1	0.75	0.19	0.29	1.26	0.84	0.93	0.71

The stress drop, $\Delta\sigma$; strain energy, E, and strain drop, Σ; are estimated using the following relations (Eshelby, 1957):

$$\Delta\sigma = \frac{3}{2}\bar{u}\,\frac{\mu n}{2r}$$

$$E = \frac{2\pi}{3\mu n} r^3 \Delta\sigma^2$$

$$\Sigma = \frac{\Delta\sigma}{\mu}$$

Here, $r = (\frac{A}{\pi})^{\frac{1}{2}}$ and $n = \frac{7}{12}\pi$

The apparent stress is a measure of the stresses acting in the focal region of the earthquake and is estimated by the following relation (Aki, 1966; Brune, 1968):

$$\eta\bar{\sigma} = \mu\,\frac{E}{M_o}$$

All these seismic source parameters are listed in Table 4.

TABLE 4. Estimates of Seismic Source Parameters

Parameters	May 30, 1935
Fault length, km	106
Fault width, km	17
Fault area, km^2	1778
Rupture velocity, km/sec	3.1
Strain energy, ergs	1.65×10^{25}
Seismic moment, dyne − cm	1.75×10^{28}
Displacement, meters	32.81
Stress drop, bars	567
Apparent stress, bars	283
Strain drop	18.9×10^{-4}
Magnitude, M (Richter, 1958)	7.6
Azimuth of strike	33°
Dip of Fault	68°NW
Slip angle	124°
Focal depth, km	20
Source time function, G (t)	$H(t)\{\log_{10}(1+\frac{a^2}{t^2})\}$

DISCUSSION

The earthquake of May 30, 1935 occurred near the Quetta syntaxis. Body and surface waves studies indicate thrust faulting along a plane with strike N 33°E, dip 68°NW and slip angle 124°. Isoseismals of maximum intensity X are aligned in the NNE direction. Chandra (1978) has determined the focal mechanism solutions for earthquakes near the Quetta region. He has obtained left-lateral strike slip faulting along the N-S striking nodal plane for one earthquake, which occurred east of Quetta. The focal mechanism solutions for earthquakes occurring near the southern part of the Sulaiman range, where the structural trend curves towards the west, shows thrust faulting along east-west or north-east striking nodal planes. The trend of the pressure axis in these mechanism solutions is slightly west of north. Near 30°N latitude, the trend of Sulaiman ranges curve around toward west in a festoon-like structure. The focal mechanism solutions determined by Chandra (1980) show predominantly strike slip faulting in this region. These solutions indicate right lateral movement along west to north-west striking nodal planes, or left lateral motion along north to north-east striking nodal planes. The seismicity trend in the epicentral region of these earthquakes favours a west to north-west striking fault plane (Quittmeyer *et al.*, 1979). Close to the epicentre of 1935 earthquake, the Jurassic rocks are overlying the Cretaceous formations and the entire formations are dipping to the north-west side. There are several thrust faults present in the region (Fig. 1) where the rocks on the northwest side of the fault have been thrusted over the rocks on the south-east side (West, 1936).

The mountains of Baluchistan consist of simple folds with axes parallel to the alignment of the mountain ranges. In general, the anticlines form the ridges and the synclines form the valleys. These folds have been formed due to relative movements between Central Asia and the Indian subcontinent. The north-south trend of the Baluchistan arc is interrupted by a sharp re-entrant angle in the neighbourhood of Quetta. At the southern end of Sulaiman range, the mountains swing sharply towards the west with an east-west trend and near Quetta, there is again a sharp bend towards the south (Fig. 1). The north-south trend is resumed along the Kirthar mountains (West, 1936). The structure of the area consists of a complex pattern of fold and thrust with axes changing from east-west to north-south.

The value of stress drop associated with the 1935 Quetta earthquake is larger than those reported for other earthquakes of similar magnitude (Abe, 1972; Ben-Menahem, 1977). The high value of stress drop and apparent stress associated with this earthquake suggests that a major part of the stresses accumulated before the occurrence of this earthquake, have been released through the main shock (Kanamori, 1972). This implies the presence of high tectonic stresses in the epicentral region of this earthquake. The Quetta region is seismically quite active.

As pointed out by Ben-Menahem and Toksöz (1962), the initial phase at the source consists of two parts: (i) the phase which is due to strain-release time function at a point on the fault, and (ii) the phase retardation due to finiteness and the motion of the source. The initial phase for the 1935 earthquake is not varying much with frequency. This implies that the above mentioned two contributions of phases are either cancelling each other or are constant along the entire frequency spectrum. Similar results were obtained in the case of Alaska earthquake of July 10, 1958 (Brune, 1961) and Chillean earthquake of May 22, 1960 (Brune *et al.*, 1961), which show a constant initial phase for the entire period range of 210 to 550 sec investigated.

CONCLUSIONS

The focal mechanism solution for earthquakes occurring in the nearby regions of Quetta syntaxis shows strike slip faulting in general. The fault plane solution for the Quetta earthquake of May 30, 1935 determined while using the body and surface waves spectral data, shows thrust faulting along a plane having strike N 33°E, dip 68°NW, slip angle 124° and a focal depth of 20 km. This earthquake is characterized by high stress drop and apparent stress; indicating that high tectonic stresses are prevailing in the epicentral region.

Acknowledgements: The authors are grateful to Dr. S. Balakrishna, Director National Geophysical Research Institute, Hyderabad, India for according permission to publish this work. The seismograms used in the present study were kindly supplied by different seismological observatories in the world. We would like to express our sincere thanks to the Directors of these observatories.

REFERENCES

Abe, K. 1972. Mechanisms and tectonic implications of the 1966 and 1970 Peru earthquakes, Phys. Earth Planet. Interiors 5, 367-379.

Aki, K. 1966 Generation and propagation of G waves from the Niigata earthquake of June 16, 1964. Part 2. Estimation of earthquake moment, released energy, and stress-strain drop from the G-wave spectrum, Bull. Earthquake Res. Inst., Tokyo Univ. 44, 73-88.

Ben-Menahem, A. 1961. Radiation of seismic surface waves from finite moving sources, Bull. Seism. Soc. Am. 51, 401-435.

Ben-Menahem, A. & Toksoz, M.N. 1962. Source-mechanism from spectra of long period seismic surface waves. 1. The Mongolian earthquake of December 4, 1957, J. Geophys. Res. 67, 1943-1955.

Ben-Menahem, A. & Toksoz, M.N. 1963. Source mechanism from spectrums of long period surface waves. 2. The Kamchatka earthquake of November 4, 1952. J. Geophys. Res. 68, 5207-5222.

Ben-Menahem, A., Aboodi, E. & Schild, R. 1974. The source of the great Assam earthquake — an interplate wedge motion, Phys. Earth Planet. Inter. 9, 265-289.

Ben-Menahem, A. 1977. Earthquake similarity laws, Phys Earth Planet. Interior 15, 10-18.

Brune, J.N. 1961. Radiation pattern of Rayleigh waves from the southeast Alaska earthquake of July 10, 1958, Symposium on Earthquake Mechanism, Pubs. Dominion Observatory, Ottawa, 24, 10, 1961.

Brune, J.N., Benioff, H. & Ewing, M. 1961. Longitudinal surface waves from the Chilean earthquake of May 22, 1960, recorded on linear strain seismographs, J. Geophys. Res. 66, 2895-2910.

Brune, J.N. 1968. Seismic moment, Seismicity and rate of slip along major fault zones, J. Geophys. Res. 73, 777-784.

Canitez, N. & Toksoz, M.N. 1971. Source parameters of earthquakes from body and surface-wave data, Bull. Seism. Soc. Am. 61, 1369-1379.

Chandra, U. 1978. Seismicity, earthquake mechanisms and tectonics along the Himalayan mountain range and vicinity, Phys. Earth Planet. Interiors 16, 109-131.

Chandra, U. 1980. Focal mechanism solutions and their tectonic implications for the Alpine-Himalayan region, east. I.C.G. Working Group 6 Volume, Am. Geophy. Union (in press).

Chinnery, M.A. 1969. Earthquake magnitude and source parameters, Bull. Seism. Soc. Am. 59, 1969-1982.

Eshelby, J.D. 1957. The determination of the elastic field of an ellipsoidal inclusion and related problems, Proc. Royal. Soc., London, A 241, 376-396.

Hagiwara, T. 1958. A note on the theory of electromagnetic seismograph, Bull. Earthquake Res. Inst. Tokyo Univ. 36, 139-164.

Harkrider, D.G. 1970. Surface waves in multilayered elastic media. Part II. Higher mode spectra and spectral ratios from point sources in plane layered earth models, Bull. Seism. Soc. Am. 60, 1937-1987.

Kanamori, H. 1972. Determination of effective tectonic stress associated with earthquake faulting: The Tottori earthquake of 1943, Phys. Earth Planet Interiors 5, 426-434.

Mills, J.M. & Hales, A.L. 1978. Great circle Rayleigh wave attention and group velocity Part II. Observations for periods between 50 and 200 seconds for nine great-circle paths and global averages for periods of 5 to 600 seconds, Phys. Earth Planet. Interiors 17, 209-231.

Quittmeyer, R.C., Farah, A. & Jacob, K.H. 1979. The seismicity of Pakistan and its relation to surface faults: in Geodynamics of Pakistan — Progress Report (eds. Abul Farah and Kees A. DeJong), Special Publication of the Geol. Survey of Pakistan, Quetta.

Richter, C.F. 1958. Elementary Seismology, W.H. Freeman, San Francisco, 768.

Singh, D.D. & Gupta, H.K. 1980. Source dynamics of two great earthquakes of the Indian sub-continent: The Bihar-Nepal earthquake of January 15, 1934 and the Quetta earthquake of May 30, 1935, Bull. Seism. Soc. Am. (in press).

Udias, A. & Arroyo, A L. 1970. Body and surface wave study of source parameters of the March 15, 1964 Spanish earthquake, Tectonophysics 9, 323-346.

West, W.D. 1936. Preliminary Geological report on the Baluchistan (Quetta) earthquake of May 31st, 1935, Rec. Geol. Survey. Ind. 69 (pt 2), 203-240.